Investigating Short Electric Field Pulses using MAVEN/LPW 2015 Observations

S. Ijaz, J.Vaverka, J. Šafránková, and Z. Němeček

Charles University, Faculty of Mathematics and Physics, Prague, Czech Republic.

Abstract. This study focuses on analyzing short (millisecond) pulses detected by the Langmuir Probe and Waves (LPW) instrument onboard the Mars Atmosphere and Volatile Evolution (MAVEN) spacecraft. We present a statistical analysis of 360,000 medium-frequency burst electric field waveforms recorded in 2015, the study aims to identify and analyze the characteristics of these transient signals. We use an automatic routine to detect waveforms with rapid fluctuations in the electric field data, this comprises over 12,000 events in the dipole and nearly 5,000 in the monopole configuration. We introduce four key parameters for event identification: the ratio of rising and decay time (t_1/t_2 or t_2/t_1) and the ratio of positive and negative part of the pulse (A_1/A_2 or A_2/A_1). The analysis particularly focuses on the dipole data, which predominantly consist of bipolar events, typically associated with dust impacts. These events are detected when the spacecraft is charged negatively and have distinct shapes that differ significantly from those recorded when the spacecraft is positively charged, indicating the influence of spacecraft's potential on the shape of the signal in dipole configuration. The peak around 200 km and the absence of events above 2000 km suggests that these pulses might not stem from interplanetary dust. We observe strong day-to-day variations in the occurrence of potential dust events, a pattern not corresponding to the Martian seasonal period or to the changes in MAVEN's orbital periapsis. Our findings contribute to the current understanding of potential dust impact signals and raises important questions regarding the influence of spacecraft's potential on detection mechanisms, interference and Electrostatic Solitary Waves (ESWs) effects in event identification, and the origin of these pulses.

Introduction

Electric field instruments are capable of detecting dust impacts on a spacecraft body as transient pulses in the measured electric field [*Aubier et al.*, 1983; *Gurnett et al.*, 1983; *Mann et al.*, 2019]. Dust impacts on the spacecraft body result in the formation of an expanding cloud of free electrons and ions, which can influence some of the scientific instruments or spacecraft's potential. The potential change can be detected by electric field instruments as transient pulses. The cosmic dust detection using electric field instruments goes back to the Voyager missions in the 1980s and their visits to Saturn, Uranus, and Neptune [*Aubier et al.*, 1983; *Gurnett et al.*, 1983; *Meyer-Vernet et al.*, 1986]. In recent times, similar electric field instruments have been used for dust detection by numerous missions in different parts of our solar system, particularly Deep Space 1 [*Tsurutani et al.*, 2004], Cassini [*Kurth et al.*, 2006; *Ye et al.*, 2016], Wind [*Malaspina and Wilson III*, 2016], STEREO [*Zaslavsky et al.*, 2012; *Kellogg et al.*, 2016], Cluster [*Vaverka et al.*, 2017a,b], Magnetospheric Multiscale (MMS) mission [*Vaverka et al.*, 2018, 2019], the Parker Solar Probe (PSP) [*Szalay et al.*, 2020; *Page et al.*, 2020] and Solar Orbiter [*Zaslavsky et al.*, 2021; *Kvammen et al.*, 2023]. Mars Atmosphere and Volatile Evolution (MAVEN) mission has detected the presence of dust at altitudes ranging from 150–1000 km [*Andersson et al.*, 2015b].

Using electric field instruments for dust impact detection offer several advantages, such as their frequent use in numerous space missions and the ability to use the entire spacecraft surface as a detector, in contrast to the limited collecting area of dedicated dust detectors. However, these instruments have limitations, as signal detection is highly dependent on the instrument's design and configuration (dipole or monopole), as well as the ambient environment, and they hardly provide any information about the impacting grains. It is important to note that not all short pulses in the data are generated by dust impacts; some may result from thrusters activity, instrumental electronics, interference with other scientific instruments, or Electrostatic Solitary Waves (ESWs). Electric field instruments in monopole configuration are known to be sensitive to potential changes on the spacecraft surface. While in dipole

configuration, dust impact signals can be registered if a plasma cloud expands asymmetrically over one of the antennas. Not all aspects of the signal generation due to an expanding plasma cloud are thoroughly understood, but recent studies have provided some explanation for it [*Nouzák et al.*, 2018; *Vaverka et al.*, 2021; *Shen et al.*, 2022]. Instruments in dipole configuration can also register direct hits on one of the electric antennas. The impact ionization process has been studied in the laboratory since 1968, an electrostatic dust accelerator was used to perform simulation experiments [*Auer and Sitte*, 1968]. Recently, the laboratory investigations of dust impacts have been carried out by using different spacecraft models [*Collette et al.*, 2015; *Nouzák et al.*, 2018; *Ye et al.*, 2019; *Shen et al.*, 2021, 2022]. These laboratory investigations, along with the theoretical models, have improved our understanding of generation of pulses after a dust impact [*Zaslavsky*, 2015; *Rackovic Babic et al.*, 2022]. Despite extensive research, we lack a comprehensive understanding of all aspects of signals generated by dust impacts in the electric field measurements. The design of the spacecraft and the dynamic space environment both play significant role in influencing the detection and interpretation of dust impact signals.

This study investigates electric field signals observed by the Langmuir Probe and Waves (LPW) instrument in both monopole and dipole configuration. We show examples of different types of short pulses detected in the Martian environment and introduce a methodology to identify signals based on their shape; however, not all of them are associated with dust impacts, and the origin of some pulses may remain ambiguous. Furthermore, we discuss the influence of spacecraft's potential on the shape and detection rate of signals likely caused by dust impacts in the dipole configuration. We analyze the altitude profiles of these events, and investigate the temporal variations and changes in ambient plasma density at lower altitudes corresponding to the varying fraction of bursts of dust events. Overall, the study provides insights into the complexity of identifying potential dust impact signals in the Martian atmosphere. It highlights the importance of considering the effects of spacecraft's potential on dust detection, and the need to distinguish interference and other waves (ESWs) from dust impact signals to avoid misinterpretation of data.

Electrostatic Solitary Waves

Electrostatic Solitary Waves (ESWs) are abundantly found in space plasma and are associated with phase space ion/electron holes [*Omura et al.*, 1999; *Pickett et al.*, 2004]. These structures arise due to localized disturbances in the plasma, resulting in a bipolar pulse in the electric field measurements [*Omura et al.*, 1999; *Graham et al.*, 2016]. The pulse duration depends on the ion/electron hole size and the relative hole-spacecraft velocity. Since the size of the spacecraft is much smaller than the ion/electron hole, the event duration is not dependent on the geometry of the spacecraft. The shape of ESWs is influenced by the orientation of the electric field antenna relative to the direction of ESWs propagation (i.e., the orientation of the magnetic field). It is highly significant that the duration and amplitudes of dust impact signals can be similar to ESWs [*Pickett et al.*, 2004; *Vaverka et al.*, 2018]. The Phobos 2 mission and recently MAVEN have shown that a significant number of bipolar electric field solitary structures and double layers are present in the Martian environment [*Grard et al.*, 1991; *Thaller et al.*, 2022; *Akbari et al.*, 2022]. These structures add complexity to the detection of dust impacts, often resulting in the false identification of dust signals and also influence the study of ESWs.

Instrument and Dataset

The MAVEN spacecraft entered into orbit around Mars on 22 September 2014, at 02:16 UT, with an orbital period ≈4.5 h. It's highly eccentric (≈0.5) and inclined (≈75°) orbit makes it possible to perform the electric field measurements around Mars between the altitudes of ≈150–6,500 km [*Jakosky et al.*, 2015]. The LPW instrument onboard MAVEN is capable of operating in two modes, as a Langmuir Probe in current mode and as an electric field instrument in waves mode. It has two nearly identical stacer booms (≈7 m). Only tips (40 cm) of the booms are sensitive to detection, this is a clear distinction from electric field instruments where the whole antenna is sensitive to dust impacts such as in Wind, STEREO, PSP and Solar Orbiter [*Bougeret et al.*, 1995; *Bale et al.*, 2008; *Maksimovic et al.*, 2020;

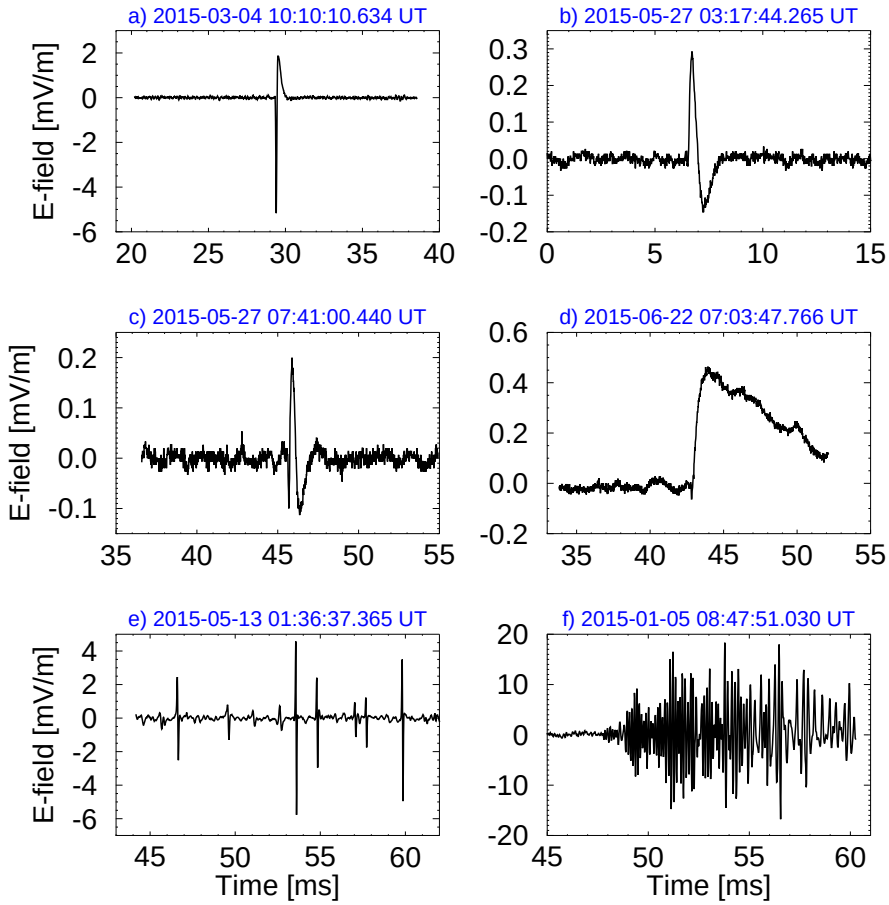

Figure 1. Examples of several waveforms recorded by LPW in dipole configuration over the year 2015. **(a,c)** shows bipolar signals with different polarities, **(d)** represents events with a pre-spike. **(e)** shows solitary wave and **(f)** is probably an electromagnetic wave. The snapshots displayed here are zoomed in to highlight distinctive features, with corresponding time stamps.

Rackovic Babic et al., 2022]. The area ratio of the spacecraft to probe surface on MAVEN is ≈100. The distance between the sensors is ≈13 m. The electric field instrument is capable of operating either in the monopole or dipole configuration. The potential drop between two cylindrical sensors located at outer ends of stacer booms is used in dipole configuration while in monopole, the potential drop between one sensor and the spacecraft is used. A clear sketch of the spacecraft and working of the instrument LPW has been described by *Andersson et al.* [2015a].

In this study, we use medium frequency burst mode data, which is one of the products obtained when the instrument records raw electric field time series in waves mode. The burst mode has a high sampling frequency for detecting dust impacts. It has three different frequency ranges with corresponding sampling rates: low frequency(1 kHz), medium frequency (65 kHz), and high frequency (4190 kHz). Among the three available frequency ranges, we use the medium frequency band as it gives closely spaced data points and long waveforms to accurately detect dust impacts. Each medium frequency (MF) burst waveform is 62.5 ms long with 4096 data points, resulting in a sampling frequency of about 65 kHz.

Events Classification and Identification

Events Classification

In our analysis, we examined nearly 360,000 medium-frequency burst waveforms from the year 2015. To identify potentially interesting events (pulses), we used an automatic routine that detects waveforms with rapid fluctuations in the measured electric field. This dataset comprises more than 12,000 events in the dipole and nearly 5,000 in the monopole configuration. We have identified various

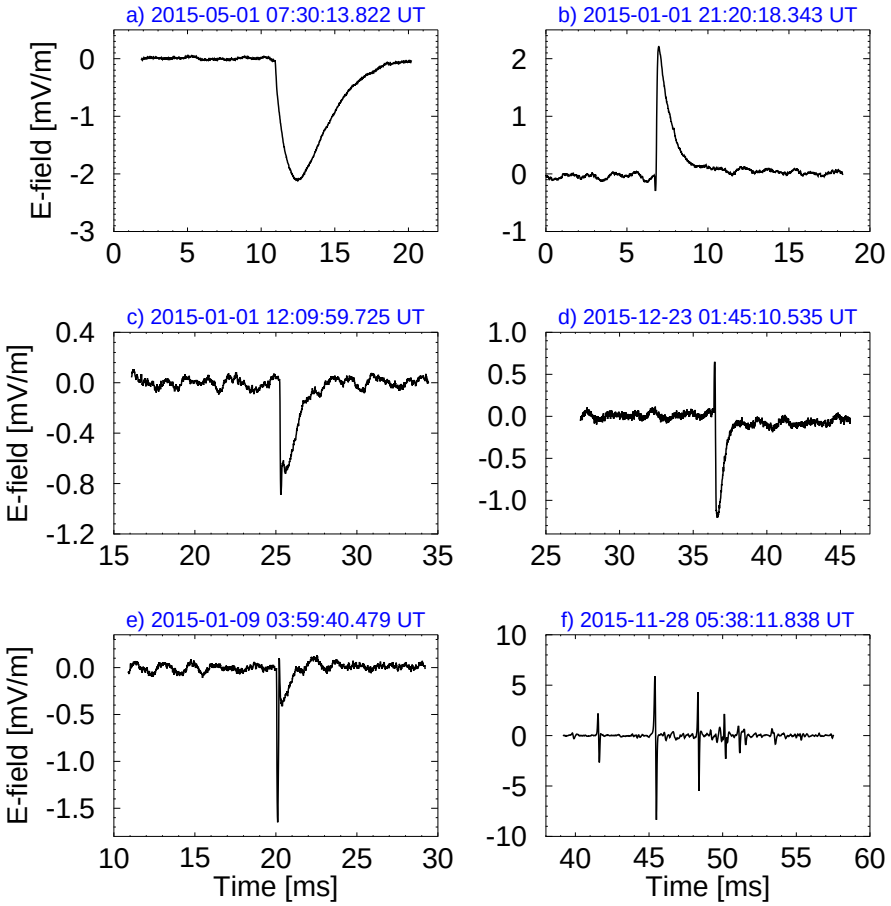

Figure 2. Same as Figure 1 but in monopole configuration. **(a)** shows an electric field signal with possibly an artificial origin, **(b)** represents single polarity events probably generated due to dust impacts. **(c,e)** shows rarely occurring events with varying pre-spike magnitudes. **(f)** shows solitary wave.

types of short pulses, though it is important to note that not all of them are associated with dust impacts, and the origin of certain pulses may remain ambiguous. In Figure 1, we illustrate examples of different event types identified by this routine over the year 2015 in the dipole configuration, and in Figure 2, we present similar examples in the monopole configuration of the electric field instrument. Additionally, in Figure 3, we showcase a selection of a few ambiguous waveforms with unknown origins, highlighting the complexity of our dataset.

Figure 1 shows various examples of events, notably, the bipolar signals shown in Figures 1a,b are predominantly detected in the ionosphere of Mars when the spacecraft has a negative potential. We observed more than 6000 such events in the dipole configuration, making them a central focus of our study. Figure 1c shows a similar bipolar event but with a pre-spike prior to the main signal. Figure 1d shows another category of events observed in the dipole configuration. The events in Figures 1c,d exhibit a pre-spike, but the initial negative spike is too rapid to be attributed to impact charge recollection. Instead, this rapid initial spike is induced by fast escaping electrons, as indicated in previous studies [*Collette et al.*, 2015; *Mann et al.*, 2019]. This pre-spike, not consistently present in all our observations, introduces an additional complexity to our understanding of these structures. Figure 1e shows an ideal example of a symmetric solitary wave. Figure 1f represents an electromagnetic wave associated with the surrounding plasma, such snapshots are excluded from our study.

Figures 2a,b showcase events recorded in the monopole configuration, characterized by a single polarity. It is observed that the counting rates of negative voltage change are 7–8 times more frequent than the counting rates of positive voltage change. Specifically, 2993 negative voltage change signals are detected at high altitudes, compared to 378 positive voltage change events. Figures 2c,d,e display rarely

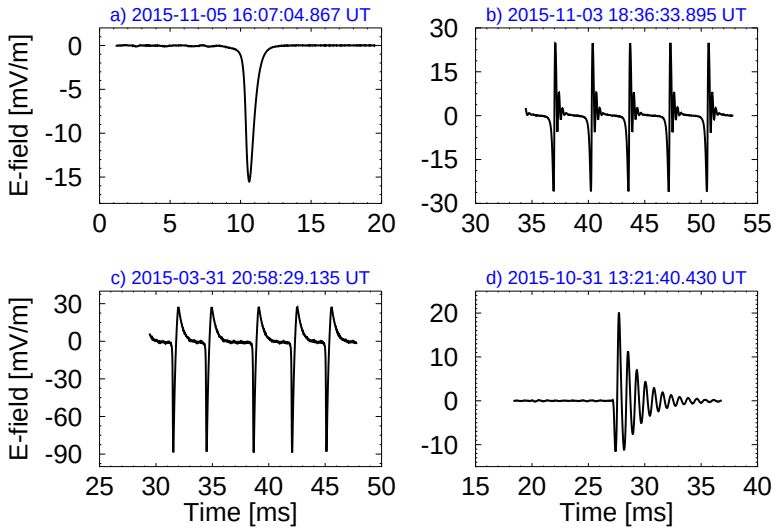

Figure 3. Examples of a few interesting ambiguous waveforms with an artificial origin, likely generated due to instrumental electronics or other such factors.

occurring events with pre-spikes of varying magnitudes. Figure 2f shows solitary wave, their detection is independent of the instrument's configuration and are therefore observed for both configurations. It is important to highlight that solitary waves can be asymmetrical contrary to the examples shown here [*Omura et al.*, 1999; *Pickett et al.*, 2004], which complicates their automatic separation from other events.

The snapshots displayed in Figures 3a,d are relatively rare. Figures 3b,c shows events that frequently occur, many of which have been automatically removed from our study. These events which might have an artificial origin have distinctive characteristics from the more common bipolar signals and other types of events in our study. Table 1 lists various parameters of electric field waveforms corresponding to dipole (Figure 1), monopole (Figure 2), and artificial events (Figure 3). t_1/t_2 is a ratio of characteristic times of the event, and A_1/A_2 is a ratio of positive and negative parts of the pulse. L_s, Lon, and Lat are the spatial coordinates. L_s refers to the solar longitude, which is a measure of the time of the Martian year that refers to the seasonal changes of the planet.

Events Identification

For reliable identification of potential dust impacts, it is essential to differentiate between structures in the ambient electric field and the variations caused by most probable dust impacts. The process of automatic identification includes several key steps:

(i) The events are selected through an algorithm by taking a threshold value for the maximum rate of change of the electric field (signal with large electric field derivation).

(ii) To remove events that are not of interest, a criterion based on the ratio of peak-to-peak amplitudes during the event to the mean absolute value of the signal prior to the event is used. Events (such as shown in Figures 1f, 3b,c) below the threshold value have been removed from the analysis. The optimal threshold value is set to be 20.

(iii) We introduce four key parameters for event identification: the ratio of rising and decay time (t_1/t_2 or t_2/t_1) and the ratio of positive and negative part of the pulse (A_1/A_2 or A_2/A_1) displayed in Figure 4. We ensured that the ratios always remain within the range 0–1 for a simpler representation.

The 2D histogram shows a visual representation of the distribution of events in the dipole (Figure 5a) and monopole (Figure 5b) configurations throughout the year 2015. The x-axis (t_1/t_2) and y-axis (A_1/A_2) in both parameter maps represent ratios of time and amplitude characteristics of events, respectively.

These ratios can be used for the identification of detected signals based on their shape. The color bar on the right side of the figures provides a logarithmic count of the total number of observations.

In the dipole configuration, the parameter map exhibits a higher logarithmic count of total observations of events, which are typically localized in nature, as indicated by red color. This localized pattern

Table 1. List of events with state parameters.

	Event Time (UTC)	t_1/t_2	A_1/A_2	L_s [deg]	Lon [deg]	Lat [deg]	Alt [km]	SZA [deg]
Dipole (Figure 1)								
(a)	2015-03-04 10:10:10.634	0.20	0.36	302	209	28	162	80
(b)	2015-05-27 03:17:44.265	0.30	0.50	349	159	–62	360	78
(c)	2015-05-27 07:41:00.440	0.39	0.57	349	246	–71	545	88
(d)	2015-06-22 07:03:47.766	0.01	0.13	2	318	17	1100	68
(e)	2015-05-13 01:36:37.365	1.00	0.79	341	204	46	1109	55
(f)	2015-01-05 08:47:51.030	1.00	0.89	266	148	–0.84	2531	51
Monopole (Figure 2)								
(a)	2015-05-01 07:30:13.822	0.03	0.02	335	222	–21	4883	148
(b)	2015-01-01 21:20:18.343	0.05	0.13	264	186	0.25	1333	132
(c)	2015-01-01 12:09:59.725	0.13	0.08	264	52	–1	1393	132
(d)	2015-12-23 01:45:10.535	0.08	0.54	85	326	47	388	86
(e)	2015-01-09 03:59:40.479	0.57	0.08	269	59	42	889	91
(f)	2015-11-28 05:38:11.838	1.00	0.79	74	41	–15	5694	113
Artificial events (Figure 3)								
(a)	2015-11-05 16:07:04.867	0.00	0.00	64	193	–37	192	65
(b)	2015-11-03 18:36:33.895	0.80	0.96	64	254	–18	161	52
(c)	2015-03-31 20:58:29.135	0.17	0.31	318	148	2	189	29
(d)	2015-10-31 13:21:40.430	0.82	0.58	62	203	–15	177	48

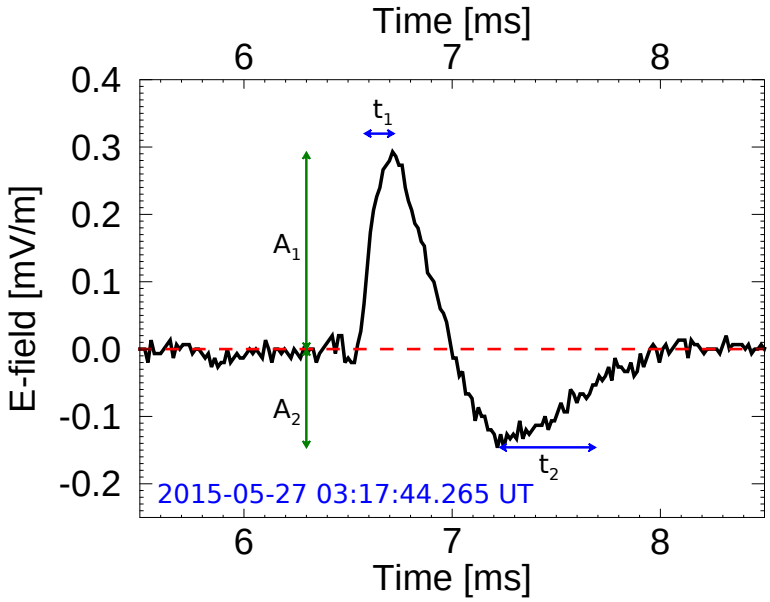

Figure 4. An example of a typical electric field waveform recorded on 27 May 2015. Key parameters of the waveform are indicated: A_1 and A_2 represent the positive and negative parts of the pulse, respectively, denoted by solid vertical lines. t_1 and t_2 correspond to rising and decay time, respectively, marked by horizontal arrows. The baseline electric field level, against which these variations are measured, is indicated by the dashed red line.

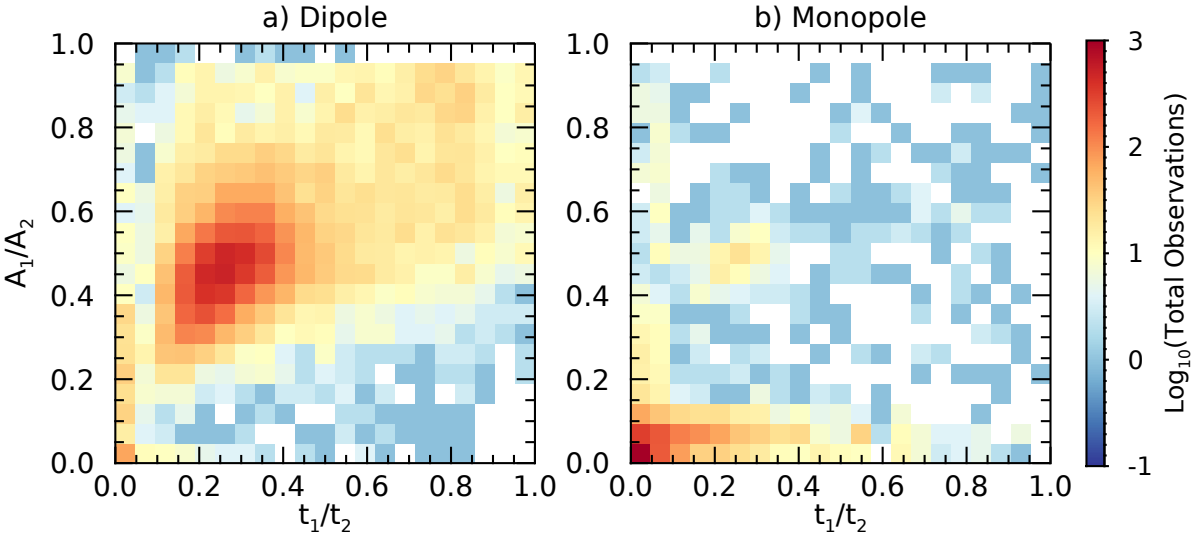

Figure 5. Parameter maps illustrating event distribution for **(a)** dipole and **(b)** monopole configurations over the year 2015. These events are color-coded using the logarithmic scale on the right.

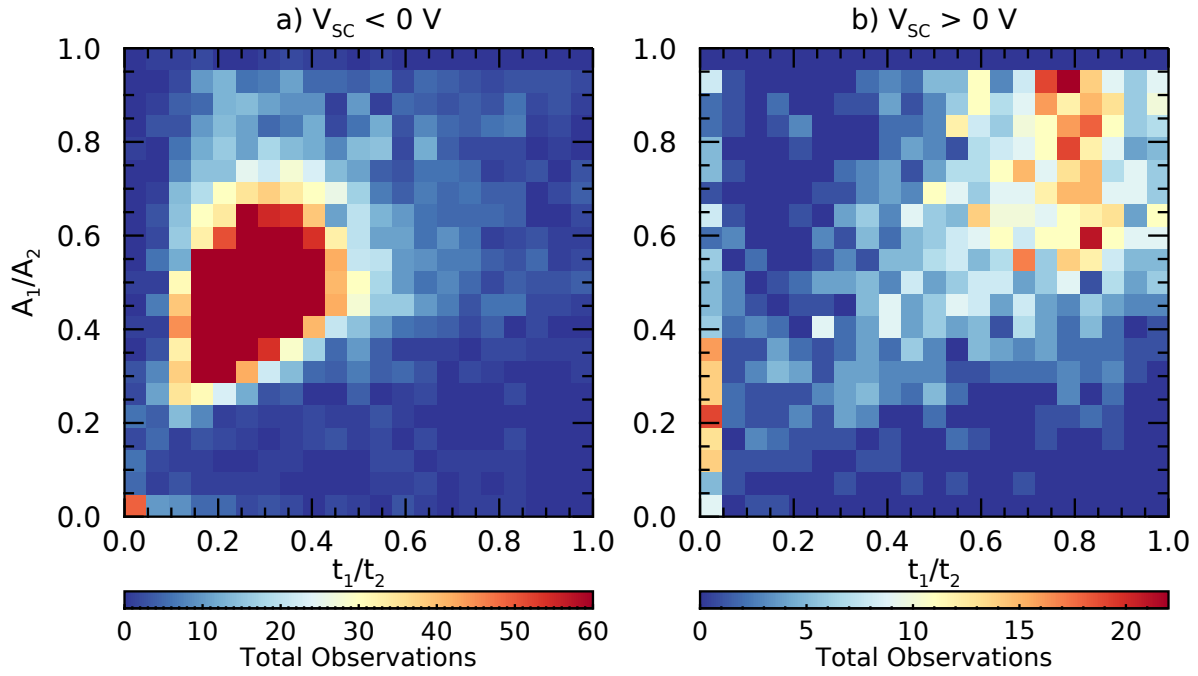

Figure 6. Parameter maps for dipole configuration under varying spacecraft potential over the year 2015. These events are color-coded using the scale at the bottom.

suggests that most of the events are within a specific range of amplitude and time ratios ($t_1/t_2 \approx 0.25$ and $A_1/A_2 \approx 0.45$), accounting for a total of nearly 7000 observed events. Another category of events constitutes background in the top-right corner of the map. These events represent mainly solitary waves, as observed in Figure 1e, with a total count of nearly 2000. The parameter map for the monopole configuration displays a localized pattern along its bottom edge, which corresponds to the events shown in Figure 2a. Additionally, there is a pattern along the left edge that relates to the pre-spike events depicted in Figure 2. This parameter map corresponds to more than 3000 single polarity events.

For MAVEN spacecraft, negative charging below 800 km altitude within Mars's ionosphere results predominantly from the collection of electrons, while positive potentials outside the dense ionosphere are due to photoemission processes. The impact of spacecraft's potential on dust detection by electric

field instruments is significant as it influences the shape and characteristics of the detected signals [*Shen et al.*, 2021].

Figure 6 provides a detailed view of Figure 5a. Figure 6a illustrates the distribution of events for a negatively charged spacecraft, while Figure 6b displays the distribution for a positively charged spacecraft over the year 2015. The 2D histograms show that the shape of pulses, as influenced by the spacecraft's potential in the dipole configuration, exhibits different patterns. For the negatively charged spacecraft, a clear concentration of events is visible in Figure 6a, where the color bar scale is adjusted to highlight less frequent occurrences by dividing the histogram values by a factor of 8. This scaling allows for the visualization of events that would otherwise be overshadowed by more common occurrences. Events with a relatively high occurrence rate are identified within the saturation region above $(\frac{1}{8})^{th}$ of the maxima 500, bins with an occurrence rate above 60 in this case. This saturation region corresponds predominantly to more than 6000 bipolar events, and notably, we observe only 500 solitary waves for the negatively charged spacecraft. Conversely, for the positively charged spacecraft in Figure 6b, events are widely spread, with pre-spike events (Figure 1d) localized on the parameter plot's left edge ($t_1/t_2 < 0.05$), and some solitary waves at the top right corner. In this case, we observe ≈200 pre-spike events and more than 1000 solitary waves. These parameter maps can be used in the automatic identification of different types of events.

Observations

The study conducted on the electric field measurements by the LPW instrument provides valuable insights into the phenomena occurring in the atmosphere near Mars. This analysis focuses on the electric field waveforms observed by MAVEN during a one-year period. By utilizing the data recorded in both the monopole and dipole configurations, the study aims to identify and analyze the characteristics of these signals. The analysis primarily focuses on the dipole configuration due to the limited availability of burst mode medium frequency data in the monopole configuration. The dataset consisting of approximately 300,000 waveforms in the dipole configuration led to the automatic detection of over 12,000 events. Our methodology indicates that observed electric field signals contain a significant number of 6000 bipolar events. These structures were observed primarily for negatively charged spacecraft in the ionosphere of Mars.

Altitude Profiles

Figure 7a shows the altitude distribution of two types of events in the dipole configuration recorded over the year 2015: most probable dust impact signals and Electrostatic Solitary Waves (ESWs), marked by red and blue respectively. The fraction of bursts (FOBs) is calculated by dividing the count of obtained events by the total number of waveforms, making it a normalized representation that considers the overall observations made by the spacecraft. These findings indicate a higher occurrence of potential dust events at lower altitudes in the ionosphere, where the spacecraft is negatively charged. The constant pattern of non-dust events (ESWs) at lower altitudes with an increase between 3,000–4,000 km indicates a distinct behavior compared to other category of events. This suggests that these two types of events may have different origins or mechanisms of formation.

Figure 7b displays a detailed view of the altitude range up to 500 km, showing a prominent peak of most probable dust events between 180–220 km, which gradually decreases below and above 200 km. The decline in the peak at lower altitudes could potentially be attributed to noise interference, which is typically encountered below 200 km. Figure 7c focuses on the influence of the spacecraft's potential (V_{SC}) on the detection of potential dust events, with the mean potential varying from positive (5 V) to negative (-5 V) as shown in the color bar. A higher fraction of bursts is detected when the spacecraft potential is below -2 V. At an altitude of 800 km, the spacecraft potential undergoes a polarity reversal, resulting in a local minimum of most probable dust events. A secondary maximum is observed at an altitude of 1200 km, corresponding to pre-spike events shown in Figure 1d, for a positively charged spacecraft and can be seen at the left edge of Figure 6b.

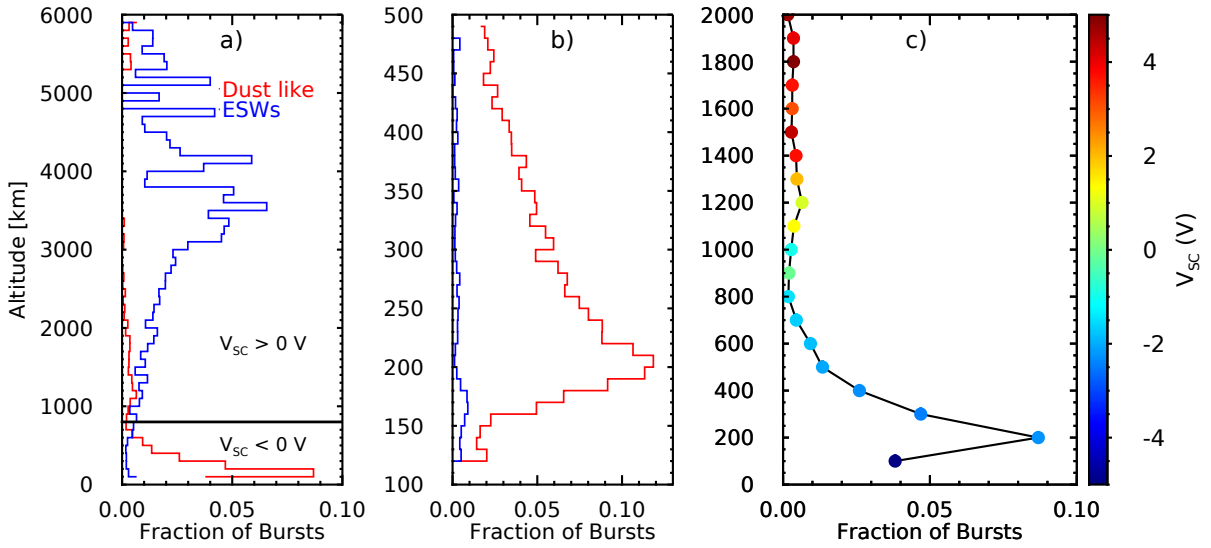

Figure 7. Fraction of bursts for the year 2015 in the dipole configuration **(a)** shows the overall altitude distribution for Dust like and ESWs events. **(b)** provides a detailed altitude profile up to 500 km. **(c)** depicts Dust like events with the color scale representing the mean spacecraft potential.

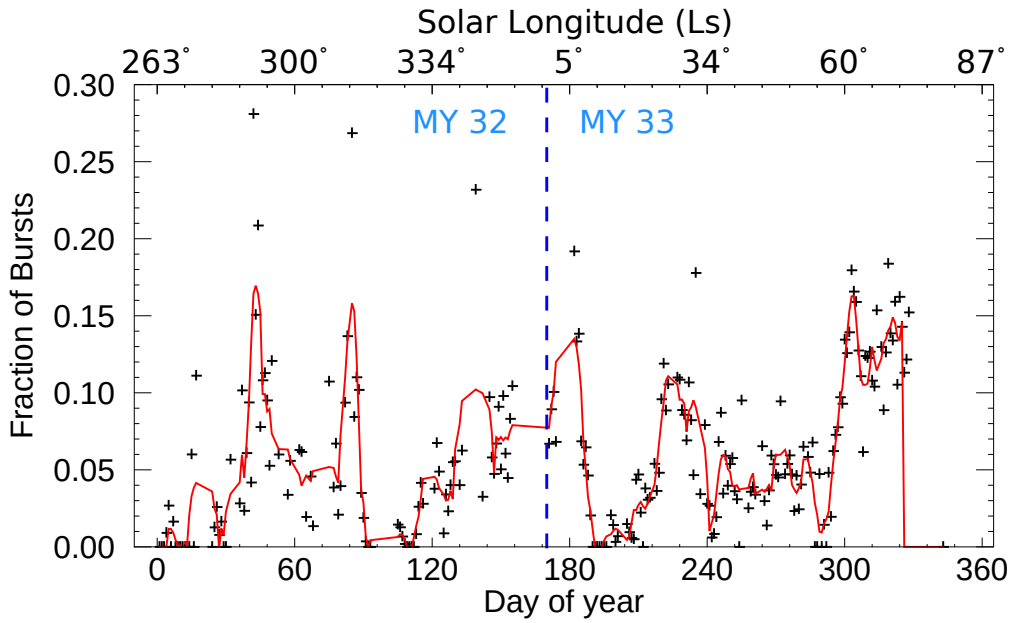

Figure 8. Fraction of bursts of potential dust candidates on Mars dayside below 500 km in the dipole configuration over the year 2015, with solar longitude (Ls) at the top. The red curve fits the individual data points.

Figure 8 depicts the daily variation in the fraction of bursts attributed to potential dust signatures throughout the year 2015 at altitudes below 500 km on the dayside of Mars. These events are detected in dipole configuration and the dashed vertical blue line represents the transition from Martian year 32 to 33. The solar longitude (Ls) marked at the top of the graph denotes the Martian seasonal period. The individual measurements are marked with '+' symbol, while the smooth red curve represents the fitted trendline, several peaks suggest periods of increased FOBs. Although we notice a considerable day-to-day variability in the fraction of bursts, it does not exhibit any seasonal variations. Furthermore, these strong temporal variations are not primarily controlled by the smooth transition of MAVEN periapsis with time, suggesting that other factors might affect their variation at Mars.

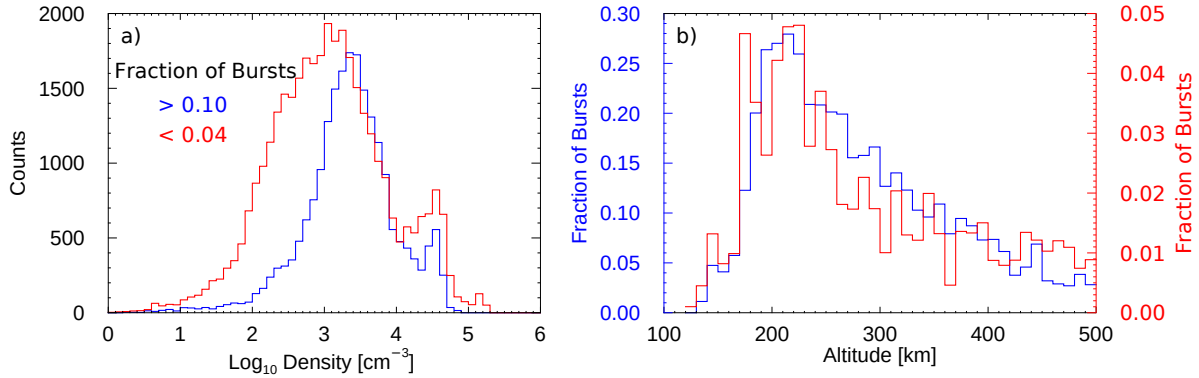

Figure 9. Histograms representing fraction of bursts above 0.10 (in blue) and below 0.04 (in red) in the dipole configuration over the year 2015 on the dayside of Mars **(a)** plasma density and **(b)** altitude profile below 500 km.

Figure 9 shows the relationship between plasma density, altitude, and the fraction of bursts that are potential dust candidates. Figure 9a presents the total observations on the dayside of Mars in the dipole configuration over the year 2015 as a function of the plasma density. The blue histogram corresponds to days when FOBs exceeds 0.10, and the red histogram represents days with FOBs below 0.04, values shown in Figure 8. There are higher counts at lower plasma densities on days with fewer FOBs ($<$ 0.04), in contrast days with greater number of FOBs ($>$ 0.10) exhibit fewer observations at these lower densities. Moreover, a similar trend can be seen for higher plasma densities, there are fewer counts for days with lesser number of FOBs ($<$ 0.04), whereas days with higher FOBs ($<$ 0.10) show more observations at these higher densities. Figure 9b provides an altitude profile for these fraction of bursts, with an altitude range of 100–500 km. It indicates that the altitude profiles are identical for varying FOBs with a peak at ≈220 km. While Figure 9 shows certain trends in the plasma density for different fraction of bursts, it is important to consider that additional factors might influence these changes, which are beyond the scope of this study.

Discussion

In this study, we analyzed more than 12,000 waveforms, consisting of both potential dust candidates and non-dust events, mainly Electrostatic Solitary Waves (ESWs). These snapshots are recorded throughout the year 2015 by the Langmuir Probe and Waves (LPW) instrument, which operates in different operation modes, either monopole or dipole. It is important to note that not all short pulses in the data are generated due to dust impacts. Some may be caused by other sources, such as thruster activity, instrumental electronics, interference with other scientific instruments, or ESWs.

The majority of probable dust events detected in the monopole configuration correspond to Figures 2a,b. These events closely resemble the typical dust impact signatures identified in various spacecraft missions and laboratory-based observations. However, these events occur in isolated groups, several hundred pulses are observed within a single hour. This count rate significantly surpasses the rates previously reported by other missions like Solar Orbiter or Parker Solar Probe. Moreover, the amplitude of these events identified within an hour are very similar, this behavior is inconsistent with impacts by dust grains of different sizes. These observations suggest that most of the events detected in the monopole configuration are probably the result of some interference, rather than the dust grain impacts on the spacecraft body.

The shape of potential dust impact signals detected in the dipole configuration varies with the spacecraft's potential (altitude). Different pulses are detected at higher altitudes, above 1000 km, where the spacecraft is positively charged. These pulses with pre-spikes are shown in Figure 1d, and are visible on the left edge of the 2D parameter map in Figure 6b. Additionally, at these higher altitudes, a significant number of ESWs are detected, these waves exhibit both polarities. At altitudes below 800 km,

where the spacecraft is negatively charged due to the denser ambient plasma environment, a significantly large number of dust impact pulses are detected. These pulses correspond to the events shown in Figures 1a,b,c and are localized within specific peak-to-peak amplitude and time ratios ($A_1/A_2 \approx 0.45$ and $t_1/t_2 \approx 0.25$), as depicted in Figure 6a. Such pulses are particularly interesting as similar events have been previously recorded by multiple spacecraft, including Wind, STEREO, MMS, Cassini, and PSP, in diverse environments, and have been interpreted as dust impacts. It is possible that the events we observe also originate from potential dust impacts, as no alternative explanations exist for such kind of pulses in electric field data. These pulses could be the result of the impact of dust grains on the spacecraft body, however, there are still some unanswered questions about their origin.

It is observed that significantly lower number of dust impact signals are detected when the spacecraft is charged positively outside the ionosphere. The current understanding of dust detection by electric field instruments does not provide any satisfactory explanation for the increased sensitivity of dipole configuration for negatively charged spacecraft. On the contrary, the increased plasma density of the ionosphere should reduce the sensitivity of the instrument in dipole configuration. Furthermore, the increase in dust event detection at lower altitudes, with a peak around 200 km, suggests that these dust grains might originate from the planet's surface. Nonetheless, there is no clear-cut explanation for the lofting of dust grains from the planet's surface up to hundreds of kilometers. *Andersson et al.* [2015b] suggested an interplanetary origin for these dust impact signals, and correlated the increased fraction of bursts at lower altitudes to the spacecraft potential. However, our extended analysis from the year 2015 does not confirm these earlier findings. Furthermore, low detection of dust impact signals outside the ionosphere questions the findings that interplanetary dust is the main source of these events. Less number of events detected below 200 km could be due to strong interference at these lower altitudes, as only events with amplitudes greater than the interference can be detected.

The occurrence of a minima in the fraction of bursts of potential dust signatures around an altitude of 800 km, where the spacecraft's potential shifts from negative to positive, is particularly interesting. A secondary smaller maximum is observed at 1200 km (Figures 7a,c). The distinct shape of the pulses along with a lower detection rate when the spacecraft is positively charged, indicates that these events might be generated by direct impacts of dust grains on the electric field sensors. This observation raises an important question regarding the absence of registered dust impacts on the spacecraft's body at altitudes exceeding 800 km. ESWs are primarily detected above 2000 km, which could be explained by the magnetopause crossing. The day-to-day variability in the fraction of bursts related to potential dust events below 500 km altitude do not correspond to the Martian seasonal period (Ls) or to the changes in MAVEN's orbital periapsis. Interestingly, altitude profiles remain identical (Figure 9b), and days with a higher fraction of bursts associate with an increased ambient plasma density (Figure 9a). The interpretation of these findings is beyond the scope of our current study.

Summary

The findings of this study highlights several key points and raises some significant questions:

(i) Langmuir Probe and Waves (LPW) instrument, operating in both monopole and dipole configurations, recorded a variety of short electric field pulses in burst mode within the Martian plasma environment. This also includes ESWs and snapshots that could be classified as interference, examples shown in Figures 1, 2, and 3.

(ii) Electrostatic Solitary Waves (ESWs) are observed in both monopole and dipole configurations of the LPW instrument, without any influence of the spacecraft potential; predominantly detected at higher altitudes likely due to magnetopause crossing.

(iii) The majority of pulses detected in the monopole configuration are probably due to some interference, though they resemble the ideal dust impact signals observed by other spacecraft and in laboratory experiments (shown in Figures 2a,b). This is supported by the fact that these events occur in large numbers, typically hundreds, with similar amplitudes in isolated groups with a one-hour duration.

(iv) Large number of potential dust events are detected within the ionosphere, where the spacecraft is charged negatively due to the dense plasma environment (Figure 7). The detection of these events significantly reduces below an altitude of 200 km, possibly due to increasing interference at lower altitudes. The absence of these events above 2000 km, depicted in Figure 7a, suggests that these pulses may not originate from interplanetary dust, contrary to the findings made by *Andersson et al.* [2015b].

(v) The shape of dust impact signals detected in the dipole configuration depends on the spacecraft's potential, which changes with altitude. We observe a decrease in the occurrence of dust events with increasing altitude, reaching a minimum at 800 km where the spacecraft potential is 0 V (as shown in Figures 7a,c).

(vi) The strong temporal variations in the occurrence of dust events cannot be explained by the Martian seasonal period (Ls) or by changes in MAVEN's orbit (periapsis), as illustrated in Figure 8.

(vii) Days when a greater fraction of bursts of dust events are observed, there is a notable increase in ambient plasma density, as indicated in Figure 9a. However, the altitude profiles below 500 km remain unaffected by the amount of the dust detected (Figure 9b).

Acknowledgments. The authors acknowledge the use of MAVEN LPW data downloaded from the Planetary Plasma Interaction Node of NASA (https://pds-ppi.igpp.ucla.edu). We also thank the LPW instrument science lead L. Andersson for the constructive comments and suggestions regarding the instrument operation. Work at the Faculty of Mathematics and Physics, Charles University is supported by the Grant Agency of Charles University (Grant No. GAUK256323). The authors would like to thank the reviewers for their valuable suggestions and comments.

References

Akbari, H., Newman, D., Fowler, C., Pfaff, R., Andersson, L., Malaspina, D., Schwartz, S., Ergun, R., McFadden, J., Mitchell, D., et al., Micro-Scale Plasma Instabilities in the Interaction Region of the Solar Wind and the Martian Upper Atmosphere, *Journal of Geophysical Research: Space Physics*, *127*, 2022.

Andersson, L., Ergun, R., Delory, G., Eriksson, A., Westfall, J., Reed, H., McCauly, J., Summers, D., and Meyers, D., The Langmuir Probe and Waves (LPW) instrument for MAVEN, *Space Science Reviews*, *195*, 2015a.

Andersson, L., Weber, T., Malaspina, D., Crary, F., Ergun, R., Delory, G., Fowler, C., Morooka, M., McEnulty, T., Eriksson, A., et al., Dust observations at Orbital Altitudes surrounding Mars, *Science*, *350*, 2015b.

Aubier, M., Meyer-Vernet, N., and Pedersen, B., Shot Noise from Grain and Particle Impacts in Saturn's Ring Plane, *Geophysical Research Letters*, *10*, 1983.

Auer, A. and Sitte, K., Detection technique for Micrometeoroids using Impact Ionization, *Earth and Planetary Science Letters*, *4*, 1968.

Bale, S. D., Ullrich, R., Goetz, K., Alster, N., Cecconi, B., Dekkali, M., Lingner, N., Macher, W., Manning, R. E., McCauley, J., et al., The electric antennas for the stereo/waves experiment, *The STEREO Mission*, pp. 529–547, 2008.

Bougeret, J. L., Kaiser, M. L., Kellogg, P. J., Manning, R., Goetz, K., Monson, S., Monge, N., Friel, L., Meetre, C., Perche, C., et al., Waves: The radio and plasma wave investigation on the wind spacecraft, *Space Science Reviews*, *71*, 231–263, 1995.

Collette, A., Meyer, G., Malaspina, D., and Sternovsky, Z., Laboratory Investigation of Antenna Signals from Dust Impacts on Spacecraft, *Journal of Geophysical Research: Space Physics*, *120*, 2015.

Graham, D. B., Khotyaintsev, Y. V., Vaivads, A., and Andre, M., Electrostatic Solitary Waves and Electrostatic Waves at the Magnetopause, *Journal of Geophysical Research: Space Physics*, *121*, 2016.

Grard, R., Nairn, C., Pedersen, A., Klimov, S., Savin, S., Skalsky, A., and Trotignon, J., Plasma and Waves around Mars, *Planetary and Space Science*, *39*, 1991.

Gurnett, D. A., Grun, E., Gallagher, D., Kurth, W., and Scarf, F., Micron-sized Particles Detected near Saturn by the Voyager Plasma Wave instrument, *Icarus*, *53*, 1983.

Jakosky, B. M., Lin, R. P., Grebowsky, J. M., Luhmann, J. G., Mitchell, D., Beutelschies, G., Priser, T., Acuna, M., Andersson, L., Baird, D., et al., The Mars Atmosphere and Volatile EvolutioN (MAVEN) Mission, *Space Science Reviews*, *195*, 2015.

Kellogg, P., Goetz, K., and Monson, S., Dust Impact Signals on the Wind Spacecraft, *Journal of Geophysical Research: Space Physics*, *121*, 2016.

Kurth, W., Averkamp, T., Gurnett, D., and Wang, Z., Cassini RPWS observations of Dust in Saturn's E Ring, *Planetary and Space Science*, *54*, 2006.

Kvammen, A., Wickstrøm, K., Kociscak, S., Vaverka, J., Nouzak, L., Zaslavsky, A., Rackovic Babic, K., Gjelsvik, A., Pisa, D., Soucek, J., et al., Machine learning Detection of Dust Impact Signals observed by the Solar Orbiter, in *Annales Geophysicae*, vol. 41, 2023.

Maksimovic, M., Bale, S., Chust, T., Khotyaintsev, Y., Krasnoselskikh, V., Kretzschmar, M., Plettemeier, D., Rucker, H., Souček, J., Steller, M., et al., The solar orbiter radio and plasma waves (rpw) instrument, *Astronomy & Astrophysics*, *642*, A12, 2020.

Malaspina, D. M. and Wilson III, L. B., A database of Interplanetary and Interstellar Dust Detected by the Wind Spacecraft, *Journal of Geophysical Research: Space Physics*, *121*, 2016.

Mann, I., Nouzak, L., Vaverka, J., Antonsen, T., Fredriksen, Å., Issautier, K., Malaspina, D., Meyer-Vernet, N., Pavlů, J., Sternovsky, Z., Stude, J., Ye, S., and Zaslavsky, A., Dust observations with Antenna measurements and its prospects for observations with Parker Solar Probe and Solar Orbiter, *Annales Geophysicae*, *37*, 2019.

Meyer-Vernet, N., Aubier, M., and Pedersen, B., Voyager 2 at Uranus: Grain Impacts in the Ring Plane, *Geophysical Research Letters*, *13*, 1986.

Nouzák, L., Hsu, S., Malaspina, D., Thayer, F., Ye, S.-Y., Pavlů, J., Němeček, Z., Šafránková, J., and Sternovsky, Z., Laboratory Modeling of Dust Impact Detection by the Cassini Spacecraft, *Planetary and Space Science*, *156*, 2018.

Omura, Y., Kojima, H., Miki, N., and Matsumoto, H., Two-Dimensional Electrostatic Solitary Waves observed by Geotail in the Magnetotail, *Advances in Space Research*, *24*, 1999.

Page, B., Bale, S. D., Bonnell, J., Goetz, K., Goodrich, K., Harvey, P. R., Larsen, R., MacDowall, R. J., Malaspina, D. M., Pokornỳ, P., et al., Examining Dust directionality with the Parker Solar Probe FIELDS instrument, *The Astrophysical Journal Supplement Series*, *246*, 2020.

Pickett, J., Kahler, S., Chen, L.-J., Huff, R., Santolik, O., Khotyaintsev, Y., Décréau, P., Winningham, D., Frahm, R., Goldstein, M., et al., Solitary Waves observed in the Auroral zone: the Cluster multi-Spacecraft perspective, *Nonlinear Processes in Geophysics*, *11*, 2004.

Rackovic Babic, K., Zaslavsky, A., Issautier, K., Meyer-Vernet, N., and Onic, D., An Analytical Model for Dust Impact Voltage Signals and its application to STEREO/WAVES data, *Astronomy & Astrophysics*, *659*, 2022.

Shen, M. M., Sternovsky, Z., Horányi, M., Hsu, H.-W., and Malaspina, D. M., Laboratory study of Antenna Signals generated by Dust Impacts on Spacecraft, *Journal of Geophysical Research: Space Physics*, *126*, 2021.

Shen, M. M., Sternovsky, Z., and Malaspina, D. M., Variability of Antenna Signals from Dust Impacts, *Journal of Geophysical Research: Space Physics*, 2022.

Szalay, J., Pokornỳ, P., Bale, S., Christian, E., Goetz, K., Goodrich, K., Hill, M., Kuchner, M., Larsen, R., Malaspina, D., et al., The near-Sun Dust Environment: initial observations from Parker Solar Probe, *The Astrophysical Journal Supplement Series*, *246*, 2020.

Thaller, S. A., Andersson, L., Schwartz, S. J., Mazelle, C., Fowler, C., Goodrich, K., Newman, D., Halekas, J., Pilinski, M. D., and Pollard, M., Bipolar Electric Field Pulses in the Martian Magnetosheath and Solar Wind; their implication and Impact accessed by system scale size, *Journal of Geophysical Research: Space Physics*, *127*, 2022.

Tsurutani, B. T., Clay, D. R., Zhang, L. D., Dasgupta, B., Brinza, D., Henry, M., Arballo, J. K., Moses, S., and Mendis, A., Plasma Clouds associated with Comet P/Borrelly Dust Impacts, *Icarus*, *167*, 2004.

Vaverka, J., Pellinen-Wannberg, A., Kero, J., Mann, I., De Spiegeleer, A., Hamrin, M., Norberg, C., and Pitkänen, T., Detection of Meteoroid Hypervelocity Impacts on the Cluster Spacecraft: First results, *Journal of Geophysical Research: Space Physics*, *122*, 2017a.

Vaverka, J., Pellinen-Wannberg, A., Kero, J., Mann, I., De Spiegeleer, A., Hamrin, M., Norberg, C., and Pitkänen, T., Potential of Earth Orbiting Spacecraft influenced by Meteoroid Hypervelocity Impacts, *IEEE Transactions on Plasma Science*, *45*, 2017b.

Vaverka, J., Nakamura, T., Kero, J., Mann, I., De Spiegeleer, A., Hamrin, M., Norberg, C., Lindqvist, P.-A., and Pellinen-Wannberg, A., Comparison of Dust Impact and Solitary Wave Signatures Detected by multiple Electric Field Antennas onboard the MMS Spacecraft, *Journal of Geophysical Research: Space Physics*, *123*, 2018.

Vaverka, J., Pavlů, J., Nouzák, L., Šafránková, J., Němeček, Z., Mann, I., Ye, S., and Lindqvist, P.-A., One-Year Analysis of Dust Impact-Like Events Onto the MMS Spacecraft, *Journal of Geophysical Research: Space Physics*, *124*, 2019.

Vaverka, J., Pavlu, J., Nouzak, L., Safrankova, J., Nemecek, Z., Antonsen, T., Mann, I., and Lindqvist, P.-A., Ion Cloud Expansion after Hyper-velocity Dust Impacts Detected by the Magnetospheric Multiscale Mission Electric Probes in the Dipole Configuration, *The Astrophysical Journal*, *921*, 2021.

Ye, S.-Y., Kurth, W., Hospodarsky, G., Averkamp, T., and Gurnett, D., Dust Detection in Space using the Monopole and Dipole Electric Field Antennas, *Journal of Geophysical Research: Space Physics*, *121*, 2016.

Ye, S.-Y., Vaverka, J., Nouzak, L., Sternovsky, Z., Zaslavsky, A., Pavlu, J., Mann, I., Hsu, H.-W., Averkamp, T., Sulaiman, A. H., et al., Understanding Cassini RPWS Antenna Signals triggered by Dust Impacts, *Geophysical Research Letters*, *46*, 2019.

Zaslavsky, A., Floating Potential Perturbations due to Micrometeoroid Impacts: Theory and application to S/WAVES data, *Journal of Geophysical Research: Space Physics*, *120*, 2015.

Zaslavsky, A., Meyer-Vernet, N., Mann, I., Czechowski, A., Issautier, K., Le Chat, G., Pantellini, F., Goetz, K., Maksimovic, M., Bale, S., et al., Interplanetary Dust Detection by Radio Antennas: Mass Calibration and Fluxes measured by STEREO/WAVES, *Journal of Geophysical Research: Space Physics*, *117*, 2012.

Zaslavsky, A., Mann, I., Soucek, J., Czechowski, A., Píša, D., Vaverka, J., Meyer-Vernet, N., Maksimovic, M., Lorfèvre, E., Issautier, K., et al., First Dust Measurements with the Solar Orbiter Radio and Plasma Wave instrument, *Astronomy & Astrophysics*, *656*, 2021.